

Classification: Biological Sciences, Biophysics.

Microscopic origins of nonlinear elasticity of biopolymer networks

J. Liu^{*}, K. E. Kasza[†], G. H. Koenderink^{†§}, D. Vader[†], C. P. Broedersz[‡], F. C. MacKintosh[‡], and D. A. Weitz^{*†¶}

^{*}Department of Physics, Harvard University, Cambridge, MA 02138, USA; [†]School of Engineering and Applied Sciences, Harvard University, Cambridge, MA 02138, USA; and [‡]Department of Physics and Astronomy, Vrije Universiteit, 1081HV Amsterdam, The Netherlands.

[§]Current address: FOM Institute for Atomic and Molecular Physics (AMOLF), 1098 SJ, Amsterdam, The Netherlands.

[¶]To whom correspondence should be addressed at: Department of Physics and School of Engineering and Applied Sciences, Harvard University, Pierce 231, 29 Oxford Street, Cambridge, MA 02138. E-mail: weitz@seas.harvard.edu.

Manuscript information:

Text: 20 pages

Figures: 5

Abstract: Cross-linked actin networks are remarkable materials with unusual mechanical properties. Their elasticity is typically highly nonlinear, exhibiting a striking increase in stiffness with strain. To elucidate the microscopic origin of this behavior, we directly image cross-linked actin networks under shear deformation. We show that the mechanism of non-linear stiffening depends on the molecular structure of the cross-linker protein. For small, rigid cross-linkers, stiffening is due to affine stretching of the actin filaments. By contrast, for large, flexible cross-links stiffening is due to non-affine filament alignment. Paradoxically, the softer cross-linkers create stronger and tougher networks.

The mechanics and dynamics of living cells are controlled in large part by the structure and elasticity of the cytoskeleton. The structure and mechanics of networks of actin, a major component of the cytoskeleton, are regulated by a myriad of actin binding proteins (ABPs), which can both cross-link and bundle actin filaments into elastic networks. These networks exhibit remarkable mechanical behavior. Unlike conventional polymer gels, they are highly elastic even for small volume fractions of protein. Moreover, their elasticity can be highly nonlinear, typically exhibiting dramatic stiffening with strain (1-5). The detailed features of this nonlinear response depend on the specific cross-linker, and, in particular, on the length and compliance of the linker domain connecting the actin-binding domains (5). Actin networks cross-linked with the large, compliant protein filamin exhibit particularly dramatic stiffening, withstanding strains up to several hundred percent and stiffening by a thousand-fold (1, 3). By contrast, actin networks cross-linked by small, rigid binding proteins, such as scruin, break at a strain of only ~30% and stiffen by at most ten-fold (2, 4). In the case of rigid linkers, the network elasticity is determined by the elastic properties of the actin filaments (2, 4). At sufficiently high cross-link density, sheared actin-scruin networks undergo uniform, or affine deformation (6-10). The network stiffening response is then due to the non-linear force-extension behavior of individual semi-flexible actin filaments (2, 11, 12). By contrast, in the case of flexible cross-linkers such as filamin, a more complicated strain-stiffening mechanism is expected, since uniform deformation is unlikely. An understanding of the origin of the mechanical behavior and the roles played by different cross-linking proteins requires quantitative imaging of the evolution of the network structure under shear. However, such experimental evidence is currently lacking.

Here, we directly visualize the network structure and structural evolution of cross-linked F-actin networks under shear deformation using a shear cell mounted on a confocal microscope. We show that networks formed with the flexible cross-linker filamin become strongly aligned in the shear direction, and that this alignment accounts for the dramatic strain-stiffening behavior of these networks. By contrast, actin networks formed with the small cross-linker scruin deform more uniformly without restructuring, and instead stiffen due to stretching of the actin filaments. Thus, the molecular structure of the cross-linker protein is critical in determining the mechanism of non-linear stiffening.

Results

Filamin A (FLNa) is the most widely expressed member of a family of F-actin cross-linking ABPs. It is a homodimer consisting of an actin-binding domain, 24 β -sheet repeats, and two unstructured sequences of 32 amino acids (13). Atomic force measurements show that, at small forces, FLNa can be modeled as a wormlike chain with a persistence length of 20 nm (14). At higher forces of 50-100 pN, the β -sheet repeat sequences reversibly unfold, doubling the total contour length (14).

For our networks, we polymerize purified rabbit skeletal muscle G-actin in the presence of human recombinant plasma gelsolin and human endothelial FLNa. We use gelsolin to control the average length of the F-actin filament to 15 μ m (15). The degree of cross-linking can be varied by changing the molar ratio of FLNa:G-actin ($R = 1/50$ - $1/1000$). To visualize the network structure at different applied strains, we label the F-actin with Alexa-488 phalloidin dye and image using confocal fluorescence microscopy.

We polymerize the networks between two parallel plates of the shear cell, which is mounted on an inverted confocal microscope, as shown by the schematic in the inset of Fig. 1A. We apply a shear strain to the network by moving the top plate with a micrometer. At each shear step, we take an image of the network structure in a plane perpendicular to the shear direction, as shown in the schematic. For an actin-filamin network with actin concentration, $c_A = 0.5$ mg/ml and $R = 1/1000$, the network consists of single undulating actin filaments and appears homogeneous and isotropic before any strain is applied, as shown in Fig. 1A. The filaments show no preferred orientation. However, when the network is subjected to step strains, the actin filaments reorient themselves and align in the direction of strain (see movie 1 in the Supplementary Information). The structure of the same network after a total strain of 100% is applied in the vertical direction is shown in Fig. 1B. Actin networks with higher concentrations of filamin ($R = 1/100$) show a different morphology in the unsheared state: thick bundles consisting of hundreds of actin filaments are embedded in a background of single filaments, as shown in the inset of Fig. 1D. Nevertheless, the network is still homogeneous and isotropic if viewed on larger length scales, as shown in Fig. 1D. After a strain of 200% is applied to this network, the originally curved bundles are straightened and similar filament alignment (Fig. 1E) is observed. Interestingly, for both the weakly (Fig. 1A-C) and strongly (Fig. 1D-F) cross-linked networks, the network structure does not recover the original isotropic state after the large applied strain is removed, as shown in Fig. 1C and 1F, respectively. Instead, the network exhibits residual local alignment and thick bundles reminiscent of the large-strain state. This hysteresis is consistent with

rheological measurements which show a slightly higher linear modulus after the network goes through a large-stress cycle (data not shown).

The strong alignment under shear can be clearly seen from the projection of confocal z -stacks onto the vertical planes shown in Fig. 2A. For a highly cross-linked and bundled sample ($c_A = 0.5$ mg/ml, $R = 1:50$), the network appears isotropic from all perspectives and the bundles are highly curved before any strain is applied, as shown in Fig. 2B. A movie showing the projection from all angles is available as movie 2 in the Supplementary Information. By contrast, with an applied strain of $\sim 200\%$, the network becomes highly aligned in the plane parallel to the shear direction and the bundles become much straighter, as shown in Fig. 2C. The network is less well aligned for planes in other directions.

To quantify filament alignment, we examine the distribution of orientation angles of the filaments at different strains for the images shown in Fig. 1. The orientation angle of the filaments is calculated by application of a local 2D moment-of-inertia filter, where pixel values of the image are equivalent to “mass” in the inertia tensor calculation, and the local orientation angle corresponds to that of the greater eigenvalue of the tensor (See the orientation angle definition in the Supplementary Information) (16). At zero strain, the distribution is flat, as shown by the solid line in Fig. 3A, indicating that the network is isotropic. With applied strain, a peak around 90° , corresponding to the direction of strain, emerges and becomes stronger with increasing strain. Based on the angle distribution, we define an orientation order parameter ω , which reflects the degree of alignment of the network, with 0 representing a perfectly isotropic network, and 1 representing a completely aligned network. A detailed definition is included in the Supplementary

Information. For the weakly cross-linked network shown in Fig. 1A-C, the orientational order parameter remains constant for strains below $\sim 30\%$, and then increases up to a strain of about 150%, as shown by the open triangles in Fig. 3B. The orientational order parameter is not exactly 0 before shear, likely due to slight alignment during sample preparation. However, the orientation angle of filaments always approaches the strain direction, 90° , at large strains independent of the initial orientation angle, as shown in Figure 1 in the Supplementary Information. To correlate the orientation behavior with the mechanical behavior, we prepare a similar network in a stress-controlled rheometer and measure its mechanical properties; these are highly non-linear. We illustrate this behavior by showing a schematic stress-strain relationship in the inset of Fig. 3C; the local slope of the stress-strain relationship is shown by the dotted line. The local slope measures the differential modulus, $K = d\sigma/d\gamma$, where σ is the stress and γ the strain (1-4). The dashed line separates the linear elastic regime, where the modulus is independent of the applied strain, and the nonlinear regime where the modulus varies as a function of strain. To measure the non-linear differential elastic modulus, we superpose a small, oscillatory stress on a static prestress on the sample, and measure the resultant oscillatory strain to determine K . To compare directly to the strain-controlled shear cell data, we plot the differential modulus as a function of the prestrain. Concomitant with the increase of the orientational order parameter, the differential elastic modulus increases by roughly three fold, as shown by the solid triangles in Fig. 3B. Similarly, for the highly cross-linked network shown in Fig. 1D-F, the sharp increase of the orientational order parameter (open squares) above a strain of about 40% is well correlated with the dramatic increase in nonlinear elasticity (solid squares), as shown in Fig. 3B.

This behavior is in sharp contrast with the behavior of actin networks cross-linked with scruin. The short and rigid scruin molecules decorate the actin filaments with scruin-scrutin interactions leading to cross-linking, and, at higher concentrations, to filament bundling (17, 18). Unlike actin-filamin networks, actin-scrutin networks show hardly any structural evolution under shear. As an example, we show mechanical data for two actin-scrutin networks in Fig. 3C, with $c_A = 0.5$ mg/ml, $R = 0.13$ (squares), and $c_A = 1$ mg/ml, $R = 0.06$ (triangles). In both cases, the differential elastic modulus increases with increasing applied strain, as shown by the solid symbols. However, the orientational order parameter hardly changes, as shown by the open symbols. Both samples break at a strain of only $\sim 30\%$. This is consistent with previous results (6, 8, 9), where actin-scrutin networks were shown to deform uniformly. Because of the uniform deformation of these networks, the strain stiffening is a result of the non-linear behavior of the individual filaments (2, 4, 11, 12).

To quantify inhomogeneous deformation and structural rearrangement under strain, we embed $1\text{-}\mu\text{m}$ -diameter particles in the network as probes. We determine their positions at strain γ_0 , as well as their corresponding positions after an incremental shear strain of $\Delta\gamma$ is applied (8). This allows us to compare their displacements with that expected from a uniform, affine strain. This is illustrated in Fig. 4A, where arrows indicate the deviation, $\Delta\vec{r}$, of filament positions (solid black line) from those expected after a uniform deformation (dotted black line). As a measure of the degree in nonaffinity, or non-uniform strain, we determine $S(\gamma_0) = \langle \Delta\vec{r}^2 \rangle / \Delta\gamma^2$, where $\langle \rangle$ denotes an average over all particles.

For actin-filamin samples, S increases significantly with increasing applied strain, for smaller strains, as shown for example for a sample with $c_A = 0.5$ mg/ml and $R = 1:100$ (squares) in Fig. 4B. At higher strains, however, the deformation becomes more and more affine. This is consistent with the evolution of both the orientational order parameter (triangles) and differential elastic modulus K' (circles). At strains below $\sim 100\%$, when the filaments and bundles are rearranging, the network deformation becomes more and more nonaffine with increasing applied strain, as measured by the increase in S , which also coincides with an increase in the orientational order parameter. In this regime, K' increases from 4 Pa to 80 Pa. A stronger increase in K' occurs at $\gamma > 100\%$; when most of the filaments and bundles are already aligned, the network deformation becomes much more affine, suggesting that the mechanical response is dominated by stretching of individual filaments and bundles. This corresponds to a strong increase in the differential elastic modulus K' from 80 Pa to 1000 Pa before breaking. Alignment is observed for all actin-filamin networks that show strain stiffening. However, the peak in the S - γ curve shifts to higher strains with decreasing cross-linking density, as shown by the circles ($R = 1:50$), squares ($R = 1:100$) and triangles ($R = 1:500$) in Fig. 4C. Since the peak indicates the maximal degree of filament reorientation, this suggests that flexible cross-linkers facilitate filament alignment and network restructuring.

The length of the actin filaments should also play an important role in network restructuring. When a filament is long, it experiences a greater torque from the surrounding filaments under shear, making alignment more effective. Conversely, as the filament length is shortened, we expect the network to restructure at larger strains, but the alignment to be less dramatic. We test these predictions by adding different

concentrations of the capping protein, gelsolin, to change the average filament length, L . For all filament lengths, the orientational order parameter increases with strain, as shown for $L = 2 \mu\text{m}$ (circles), $5 \mu\text{m}$ (triangles) and $10 \mu\text{m}$ (squares) in Fig. 5. However, for the network with the longest average filament length, $L = 10 \mu\text{m}$, the alignment is the most dramatic and occurs at the smallest strain. This is consistent with large amplitude sweep test from bulk rheology experiments, as shown in the inset of Fig. 5. Stiffening is observed for all filament lengths, as shown for $L = 5 \mu\text{m}$ (triangles), $7 \mu\text{m}$ (stars), $10 \mu\text{m}$ (squares), $15 \mu\text{m}$ (diamonds). However, with increasing L , the stiffening becomes more dramatic and occurs at smaller strains (19). This inverse relationship of critical strain with average filament length is consistent with a simple model of networks consisting of stiff actin filaments decorated with flexible crosslinkers of maximum extension $\ell_0 < L$, in which the critical strain $\gamma_c \cong \ell_0 / L$ for the onset of nonlinearity (19, 20) (see Supplementary Information). Experiments using engineered crosslinks of varying length ℓ_0 have shown the linear dependence of critical strain on ℓ_0 , expected within this model (5).

Discussion

We have demonstrated that actin networks cross-linked with filamin A exhibit dramatic filament alignment upon shearing, as shown by both the increase in orientational order parameter (Fig. 3B) and in the nonaffinity (Fig. 4B), which indicates significant structural rearrangement of the network. This restructuring is made possible in part because the filamin cross-linkers are large, compliant molecules: Local restructuring and reorientation of actin filaments relative to their neighbors result in a large fraction of filaments and

bundles aligned in the direction of strain at large applied strains (Fig. 2*B*). Further shearing of the network effectively stretches this collection of filaments and bundles. This large-strain stretching regime coincides with the most dramatic macroscopic strain stiffening. Moreover, since the filamin cross-linkers are compliant, they increase the network compliance beyond that of the actin filaments alone; this leads to a very high breakage strain.

The behavior of actin-filamin networks is in marked contrast with the more limited structural rearrangements of actin networks cross-linked with rigid actin binding proteins such as scruin. Upon shearing, actin-scrutin networks deform more uniformly, as confirmed by both the orientational order parameter (Fig. 3*C*) and nonaffinity measure (8). This is consistent with the fact that scruin cross-linkers are rigid and permanent; their lack of compliance prevents both local network rearrangement and large macroscopic strains. This uniform deformation leads to strain stiffening at smaller strains reflecting the stretching of individual actin filaments, which have a non-linear force-extension relation, typical of semi-flexible filaments (2, 12). However, since the corresponding strain is smaller and more uniform, the stress induced by shearing is effectively concentrated in a small fraction of filaments oriented at 45° relative to the shear direction (4). This reduces the maximum stress that the network can support. Also, given their more rigid initial state, at the same concentration of cross-linkers, actin-scrutin networks exhibit smaller relative stiffening than actin-filamin networks.

The structural rearrangement of actin-filamin networks under shear shows hysteresis upon removal of the strain (Fig. 1*C* and *F*). The network structure does not completely recover to the original isotropic state, but shows residual local alignment and

bundling. This strongly suggests unbinding of the dynamic filamin cross-linkers at high strains and rebinding to neighboring sites. This observation is consistent with rheological measurements which show a higher linear modulus after the network is subjected to a large stress cycle, a phenomenon known as work-hardening. By contrast, neither hysteresis nor work-hardening is observed in actin-scrutin networks. Instead, actin-scrutin networks are completely reversible in both network structure and rheology, in accordance with the high binding affinity of scrutin for actin.

By directly visualizing the structural evolution of cross-linked and bundled actin networks under shear deformation, we are able to identify the micro-structural origins of the striking nonlinear mechanical properties of actin-filamin networks. We also see how actin-filamin networks are able to withstand larger shear stresses and even become stiffer than actin networks formed with stronger actin-binding proteins. Paradoxically, this added strength-toughness of actin-filamin networks is made possible by the softer, more compliant nature of the filamin. This shows the essential synergistic nature of these composite networks: through the combination of stiff and flexible elements, the cellular cytoskeleton can achieve enhanced load-bearing capacity, while remaining compliant. This can have important implications for the design of synthetic polymeric materials that have these seemingly incompatible elastic properties. Indeed, the techniques introduced here can also be used to study the micro-structural basis of mechanics in other biopolymer networks.

Materials and Methods

Protein Preparation. Actin is purified from rabbit skeletal muscle, using a gel filtration column to remove capping and cross-linker proteins. Recombinant human gelsolin is produced in *Escherichia coli* (21). Recombinant FLNa is purified from Sf9 cell lysates (22). Scrutin is purified from the acrosomal process of *Limulus* sperm (23, 24). All proteins are rapidly frozen in liquid nitrogen, and stored at -80°C .

***In vitro* Network Formation.** To form *in vitro* networks, solutions of G-actin, gelsolin, Filamin A or scrutin are gently mixed and $10\times$ actin polymerization buffer (2 mM Tris·HCl/2 mM MgCl_2 /100 mM KCl/0.2 mM DTT/0.2 mM CaCl_2 /0.5 mM ATP, pH 7.5) is added last. The solution is loaded immediately into the shear cell, surrounded by mineral oil to prevent drying, and incubated for 1 hour at 25°C . By varying the gelsolin concentration relative to actin concentration, c_A , the average filament length, L , can be varied (15). By varying the molar concentration of cross-links, c_{xlink} , relative to c_A , the degree of cross-linking and bundling is varied; we define $R = c_{\text{xlink}}/c_A$.

Shear Cell. The shear cell is mounted on an inverted confocal microscope (8). The sample is sheared between a fixed bottom cover slip and a movable top plate, 6 mm in diameter. The gap is $\sim 500\ \mu\text{m}$ and the plates are parallel to within $1\ \mu\text{m}$ over the shear zone. A micrometer moves the top plate, which is parallel to the focal plane.

Network Structure Visualization. Confocal fluorescence microscopy is used to visualize the structure of the cross-linked and bundled F-actin network. We deposit a $1\text{-}\mu\text{l}$ drop of $33\ \mu\text{M}$ Alexa 488 phalloidin (catalog no. A12379, Invitrogen) in methanol into a centrifuge tube, and allow it to dry completely. In this tube, we mix the sample as described above, and load the labeled sample into the shear cell. The sample is examined with a Zeiss LSM 510-Meta confocal microscope. Laser excitation at 488 nm is used

with a LP 505 filter and HFT 488/543 beam splitters. For the 3D imaging shown in Fig. 3, a z-stack of 200-300 frames was collected with an interval of 300 nm between adjacent slices. A 3D projection was reconstructed using the Zeiss software.

Bulk Rheology. The bulk mechanical response of the networks is measured with a stress-controlled rheometer (G2, TA Instruments) with a cone-plate geometry. We superpose a small, oscillatory stress on a static prestress, and measure the resultant oscillatory strain to determine differential moduli K' and K'' (1, 2, 4). The prestrain corresponding to the prestress is calculated from the angular position of the tool.

Nonaffinity. To measure nonaffinity, we embed in the network fluorescent yellow-green carboxylate-modified latex particles of diameter $1 \mu\text{m}$ (catalog no. F8823, Invitrogen) as probes (8). At each applied strain γ_0 , we first collect several images of a single plane and confirm the absence of slip or drift. Then a z-stack of 121 frames containing ~ 200 particles is collected with an interval of 300 nm between adjacent slices. We determine the 3D positions of the centers of particles (25, 26) at γ_0 , and their corresponding positions after a shear increment $\Delta\gamma$ is applied, with a resolution of $\sim 0.02 - 0.1 \mu\text{m}$, depending on network stiffness, and limited by thermal motion. The particle displacement in the strain direction, Δy , is linear with height, z , as shown in Figure 2 in the Supplementary Information. This confirms that the average strain is affine, enabling us to determine the strain increment applied to the sample, $\Delta\gamma$, from a fit to the displacement profile. The positions of the particles after a perfectly affine deformation are calculated from this $\Delta\gamma$. The deviation of the actual positions of particles from their

affine positions is $\Delta\vec{r}$. The differential nonaffinity measure at γ_0 is calculated as

$$S(\gamma_0) = \langle \Delta\vec{r}^2 \rangle / \Delta\gamma^2, \text{ where } \langle \rangle \text{ denotes averaging over all particles (10).}$$

We thank F. Nakamura for preparation of actin, gelsolin and filamin, G. Waller for assistance with scruiin purification, and L. Jawerth for discussions. This work was supported by the NSF (DMR-0602684, CTS-0505929), the Harvard MRSEC (DMR-0213805), and the Foundation for Fundamental Research on Matter (FOM). GHK was supported by a European Marie Curie Fellowship (FP6-2002-Mobility-6B, Contract No. 8526). The confocal microscope is maintained by the Harvard Center for Nanoscale Systems.

References

1. Gardel, M. L., *et al.* (2006) Prestressed F-actin networks cross-linked by hinged filamins replicate mechanical properties of cells. *Proc. Natl. Acad. Sci. USA* 103: 1762-1767.
2. Gardel, M. L., *et al.* (2004) Elastic behavior of cross-linked and bundled actin networks. *Science* 304: 1301-1305.
3. Gardel, M. L., *et al.* (2006) Stress-Dependent Elasticity of Composite Actin Networks as a Model for Cell Behavior. *Phys. Rev. Lett.* 96: 088102.
4. Gardel, M. L., *et al.* (2004) Scaling of F-Actin Network Rheology to Probe Single Filament Elasticity and Dynamics. *Phys. Rev. Lett.* 93: 188102.
5. Wagner, B., Tharmann, R., Haase, I., Fischer, M. & Bausch, A. R. (2006) Cytoskeletal polymer networks: molecular structure of crosslinkers determine macroscopic properties. *Proc Natl Acad Sci USA* 103: 13974-13978.
6. Head, D. A., Levine, A. J. & MacKintosh, F. C. (2003) Distinct regimes of elastic response and deformation modes of cross-linked cytoskeletal and semiflexible polymer networks. *Phys. Rev. E* 68: 061907.
7. Head, D. A., Levine, A. J. & MacKintosh, F. C. (2003) Deformation of cross-linked semiflexible polymer networks. *Phys. Rev. Lett.* 91: 108102.
8. Liu, J., Koenderink, G. H., Kasza, K. E., MacKintosh, F. C. & Weitz, D. A. (2007) Visualizing the strain field in semiflexible polymer networks: strain fluctuations and nonlinear rheology of F-actin gels. *Phys. Rev. Lett.* 98: 198304.
9. Wilhelm, J. & Frey, E. (2003) Elasticity of Stiff Polymer Networks. *Phys. Rev. Lett.* 91: 108103.
10. Onck, P. R., Koeman, T., Dillen, T. v. & Giessen, E. v. d. (2005) Alternative explanation of stiffening in cross-linked semiflexible networks. *Phys. Rev. Lett.* 95: 178102.
11. Storm, C., Pastore, J. J., MacKintosh, F. C., Lubensky, T. C. & Janmey, P. A. (2005) Nonlinear elasticity in biological gels. *Nature* 435: 191-194.
12. MacKintosh, F. C., Kas, J. & Janmey, P. A. (1995) Elasticity of semiflexible biopolymer networks. *Phys. Rev. Lett.* 75: 4425-4428.
13. Stossel, T. P., *et al.* (2001) Filamins as integrators of cell mechanics and signalling. *Nat. Rev. Mol. Cell Biol.* 2: 138-145.

14. Furuike, S., Ito, T. & Yamazaki, M. (2001) Mechanical unfolding of single filamin A (ABP-280) molecules detected by atomic force microscopy. *FEBS Lett.* 498: 72-75.
15. Janmey, P. A., Peetermans, J., Zaner, K. S., Stossel, T. P. & Tanaka, T. (1986) Structure and mobility of actin filaments as measured by quasielastic light scattering, viscometry, and electron microscopy. *J. Biol. Chem.* 261: 8357-8362.
16. Vader, D., Kabla, A., Mahadevan, L. & Weitz, D. A. (2007) Strain-induced alignment in elastic collagen gels. *to be published.*
17. Schmid, M., Agris, J., Jakana, J., Matsudaira, P. & Chiu, W. (1994) Three-Dimensional Structure of a Single Filament in the Limulus Acrosomal Bundle: Scruin Binds to Homologous Helix-Loop-Beta Motifs in Actin. *J. Cell Biol.* 124: 341-350.
18. Sherman, M., *et al.* (1999) The Three-Dimensional Structure of a Dynamic Actin Bundle, the Limulus Acrosomal Process. *J. Mol. Biol.* 294: 139-149.
19. Kasza, K. E., *et al.* (2007) Elastic regimes of stiff biopolymers connected by flexible linkers. *to be published.*
20. Broedersz, C. P., Storm, C. & MacKintosh, F. C. (2007) Nonlinear elasticity of composite networks of stiff biopolymers with flexible linkers. *arXiv:0710.3951v1 [cond-mat.soft]*.
21. Kwiatkowski, D. J., Janmey, P. A. & Yin, H. L. (1989) Identification of critical functional and regulatory domains in gelsolin. *J. Cell Biol.* 108: 1717-1726.
22. Nakamura, F., Osborn, E., Janmey, P. A. & Stossel, T. P. (2002) Comparison of Filamin A-induced Cross-linking and Arp2/3 Complex-mediated Branching on the Mechanics of Actin Filaments. *J. Biol. Chem.* 277: 9148-9154.
23. Schmid, M. F., *et al.* (1991) Crystallographic Analysis of Acrosomal Bundle from Limulus Sperm. *J. Mol. Biol.* 221: 711-725.
24. Shin, J. H., Mahadevan, L., Waller, G., Langsetmo, K. & Matsudaira, P. (2003) Stored elastic energy powers the 60 micrometre extension of the Limulus polyphemus sperm actin bundle. *J. Cell Biol.* 162: 1183-1188.
25. Crocker, J. C. & Grier, D. G. (1996) Methods of digital video microscopy for colloidal studies. *J. Colloid Interface Sci.* 179: 298-310.
26. Liu, J., *et al.* (2006) Microrheology probes length scale dependent rheology. *Phys. Rev. Lett.* 96: 118104.

Figure captions

Fig. 1. Morphology of actin-filamin networks during different stages of shearing. The images are taken in a plane parallel to the two shearing plates and the focal plane, as sketched in the inset of (A). (A-C) A weakly cross-linked sample ($c_A = 0.5$ mg/ml, $R = 1:1000$). (Scale bar = $20 \mu\text{m}$.) (A) At zero strain, the network appears homogeneous and the undulating single filaments show no preferred orientation. (B) At strain 100%, the filaments are aligned in the direction of shear, as indicated by the arrow. (C) Upon removal of the strain, the network does not completely recover to its original, isotropic, state. (D-F) A highly cross-linked and bundled sample ($c_A = 0.5$ mg/ml, $R = 1:100$). (Scale bar = $50 \mu\text{m}$.) (D) At zero strain, the network consists of thick bundles embedded in a background of single filaments, most clearly seen in the higher magnification image in the inset (Scale bar = $20 \mu\text{m}$). However, the network is still isotropic. (E) At strain 200%, the filaments and bundles become strongly aligned in the shear direction. (F) When returned to zero strain, the network does not recover to the isotropic state; instead, it retains some local alignment and thick bundles, reminiscent of the large-strain state.

Fig. 2. Network structure in 3D for a highly cross-linked and bundled sample, $c_A = 0.5$ mg/ml, $R = 1:50$. About 270 images with 300-nm intervals are assembled and projected onto the vertical planes, as shown in (A). The movie is available as Supplementary Information. (B) Network structure at strain 0 viewed from the angles shown in (A). The network appears isotropic and the bundles are wavy before shearing. (C) Network structure at strain 200% viewed from the angles shown in (A). After shearing, the bundles are straightened and highly aligned in the shear direction.

Fig. 3. Correlation between orientational order parameter and nonlinear rheology. (A) The orientation angle distribution for all filaments in actin-filamin network with $R = 1:1000$ at strains 0 (solid), 53% (dash), 132% (dot), 185% (dash-dot). (B) The increase of the orientational order parameter (open symbols) with increasing strain is well correlated with the increase of the differential elastic modulus (solid symbols) for actin-filamin networks with $R = 1:1000$ (triangles) and $R = 1:100$ (squares). The differential elastic modulus is a robust measure of the nonlinear elasticity. It is obtained by superposing a small, oscillatory stress on a static prestress, and measuring the resultant oscillatory strain. Therefore, it is equivalent to measuring the local slope of the stress-strain curve, as shown by the dotted line in the inset of (C). In the linear regime, which is to the left of the vertical dashed line, the differential modulus measures the linear modulus. (C) For two actin-scruin networks (squares: $c_A = 0.5$ mg/ml, $R = 0.13$; triangles: $c_A = 1$ mg/ml, $R = 0.06$), the differential elastic modulus (solid symbols) increases with increasing applied strain, while the orientational order parameter (open symbols) hardly changes. Both samples break at a strain of only $\sim 30\%$.

Fig. 4. The degree of deviation from uniform deformation during straining. (A) Schematic showing the deviation of the position of a filament (solid black line) from that expected after a uniform deformation (dotted black line). Arrows show the deviation distance that is measured. (B) The differential nonaffinity measure S (squares) evolves non-monotonically with strain for a highly cross-linked and bundled sample with $c_A = 0.5$ mg/ml, $R = 1:100$. At strains below $\sim 100\%$, when the filaments and bundles are

rearranging, the network deformation becomes more and more nonaffine with increasing applied strain, consistent with the increase in orientational order parameter (triangles). In this regime, the stiffening is not as strong as at $\gamma > 100\%$ (circles). At strains above 100%, when all the filaments and bundles are aligned, the network deformation becomes much more affine and dominated by stretching of individual filaments and bundles. This corresponds to a sharp increase in the differential elastic modulus. (C) The S - γ curve for actin-filamin samples with different cross-linking density, $R = 1:50$ (circles), $R = 1:100$ (squares), $R = 1:500$ (triangles). A similar pattern is observed for all actin-filamin networks that show strain stiffening, but the peak in the S - γ curve shifts to higher strains when the cross-linking density decreases. Since the peak indicates the maximal degree of filament reorientation, this suggests that flexible cross-linkers facilitate filament alignment and network restructuring.

Fig. 5. Evolution of orientational order parameter under strain for actin-filamin network ($c_A = 0.5$ mg/ml, $R = 1:100$) with different average filament length, $10 \mu\text{m}$ (squares), $5 \mu\text{m}$ (triangles) and $2 \mu\text{m}$ (circles). The inset shows the large amplitude sweep test for the same samples with different average filament length, $15 \mu\text{m}$ (squares), $10 \mu\text{m}$ (circles), $7 \mu\text{m}$ (up triangles), and $5 \mu\text{m}$ (down triangles). The elastic modulus G' has been scaled by the linear modulus, G_0 .

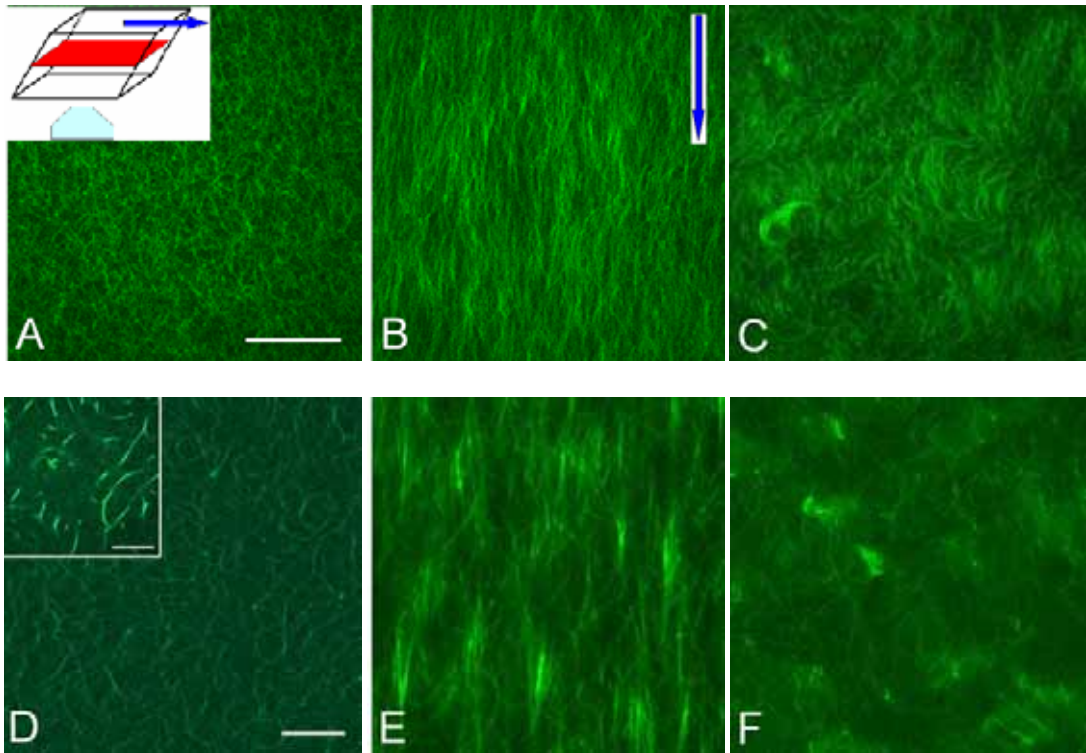


Figure 1

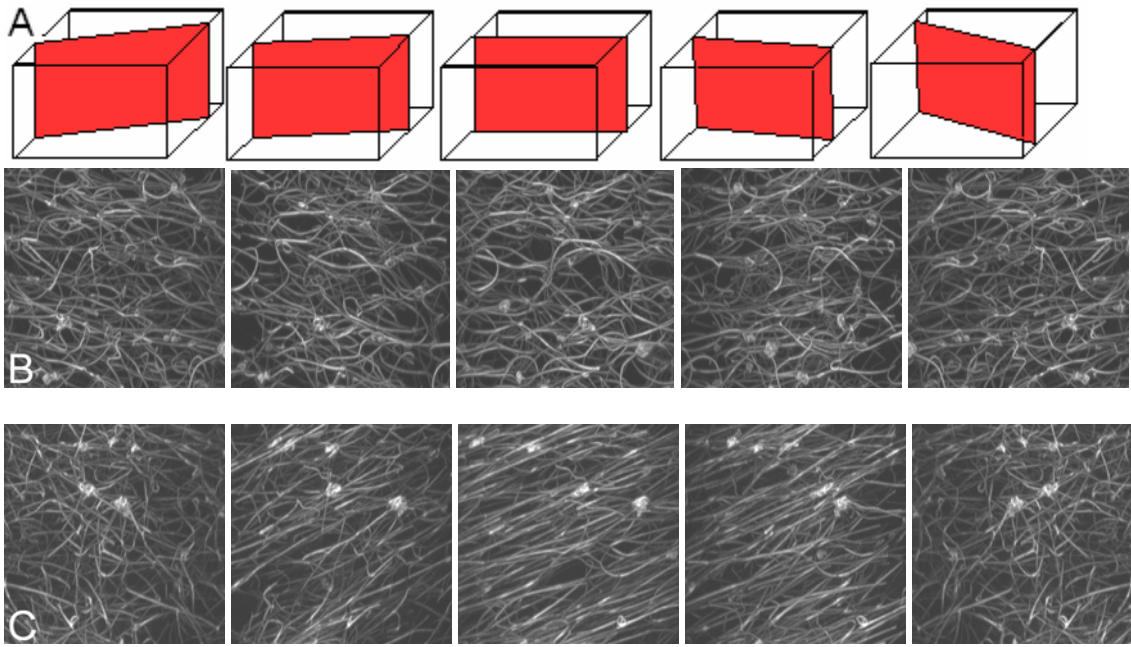


Figure 2

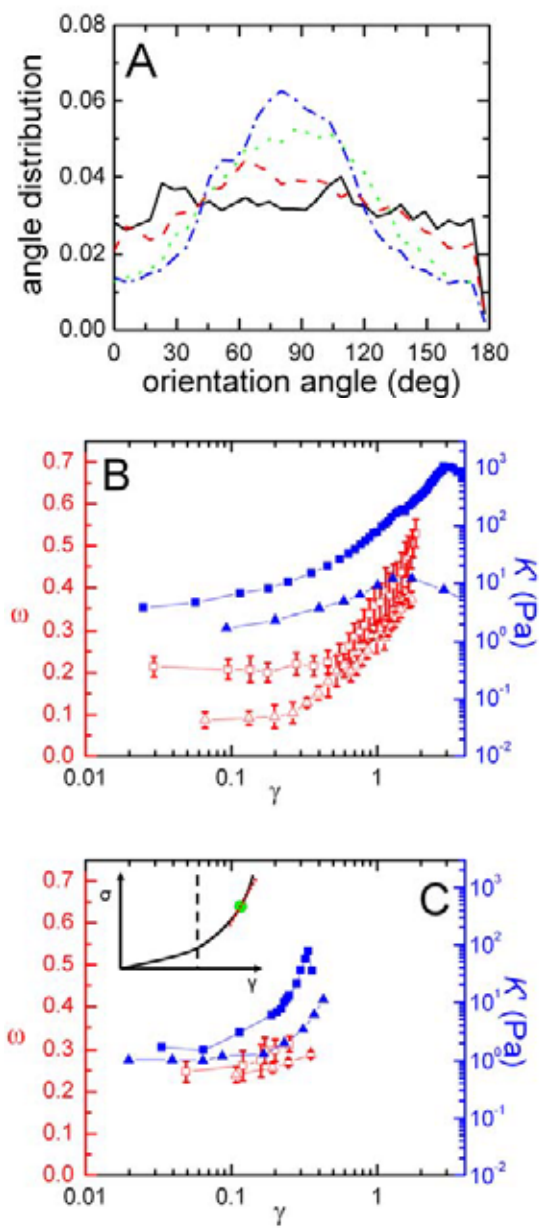


Figure 3

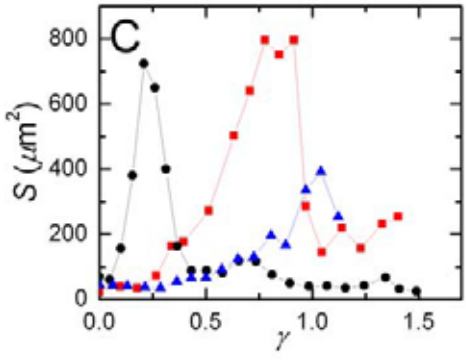
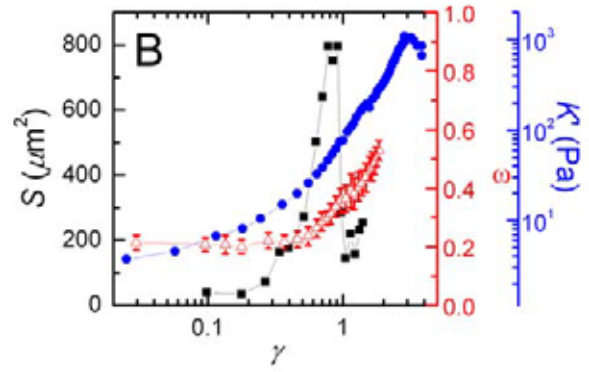
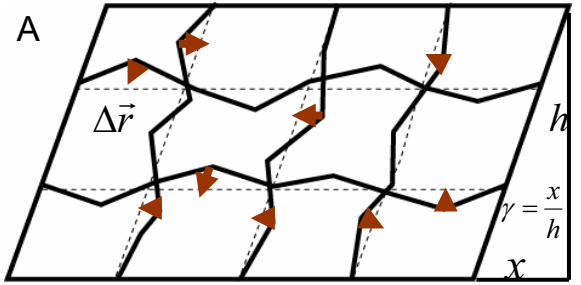


Figure 4

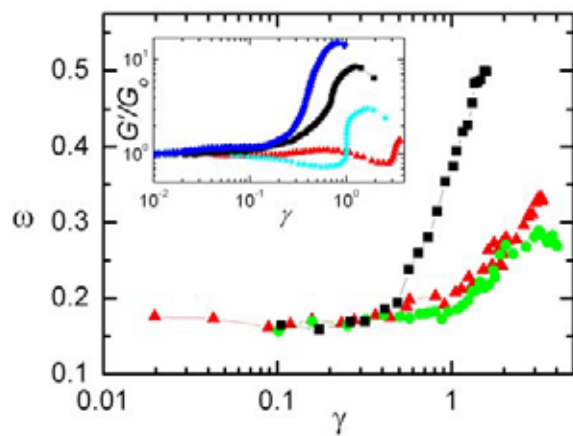


Figure 5